

Quantum-noise reduction at frequencies up to 0.5 GHz using pulsed parametric amplification

Paul D. Townsend and Rodney Loudon*

BT Laboratories, Martlesham Heath, Ipswich IP5 7RE, United Kingdom

(Received 30 May 1991)

Measurements of quantum-noise reduction have been performed over a broad frequency range up to 0.5 GHz using pulses of squeezed light generated by parametric amplification in KTiOPO_4 crystals. Both balanced-homodyne and direct-difference photodetection schemes were employed, and 0.5 dB of noise reduction was routinely obtained. A continuous-mode traveling-wave theory including the effects of dispersion and loss has been employed to model the experimental results.

PACS number(s): 42.50.Dv, 42.50.Lc, 42.65.Ky

I. INTRODUCTION

The quantum-mechanical description of light predicts the presence of noise in the optical field that ultimately limits the sensitivity of optical communication systems and spectroscopic measurements in general. This “vacuum” or “shot” noise arises from the noncommutability of the quadrature-electric-field operators, and it leads to fundamental fluctuations in the two quadrature-field components via the uncertainty principle [1]. It is now well established that certain nonlinear effects, such as four-wave mixing [2,3] and parametric amplification [4–7], can be used to decrease (squeeze) the vacuum noise in one field quadrature at the expense of increased noise in the other quadrature. Hence, by using squeezed light, precision measurements below the shot-noise limit have been demonstrated [8–10]. Parametric amplification has been perhaps the most widely used technique to date, and measurable degrees of squeezing have been obtained in continuous-wave experiments by enclosing the nonlinear medium in an optical cavity to enhance the interaction length [4,8–10] or, alternatively, by using intense pulses in a traveling-wave amplifier format [5–7]. One advantage of the latter approach is that the frequency bandwidth over which squeezing occurs is not limited by the cavity storage time, and it can therefore be of the order of the phase-matching bandwidth of the nonlinear crystal, which may be in the terahertz range. In this work we have used pulsed parametric amplification in KTiOPO_4 (KTP) crystals to investigate both quadrature squeezing via phase-sensitive homodyne detection, and also “twin-beam” noise reduction using direct-detection techniques [11–13]. By an appropriate choice of detector electronics we were able to measure squeezing up to very high frequencies of ~ 0.5 GHz with typical noise reductions of 0.5 dB (11%). The modest levels of noise reduction were sufficient to investigate some of the underlying physics of the squeezing process, and in order to do this we also carried out a coordinated theoretical study. In particular, a multimode traveling-wave theory of the parametric amplifier was developed that included the effects of polar-

ization, dispersion, and loss. By comparing experiment and theory, we determined values for the key parameters such as gain and mode mismatch in the model, and also investigated the effects of loss on the observed quantum properties.

II. EXPERIMENTAL DETAILS

The apparatus used for the squeezing experiments is shown schematically in Fig. 1. The optical source is a mode-locked neodymium-doped yttrium lithium fluoride (Nd:YLF) laser which operates at a wavelength of 1053 nm in the near infrared, and produces 50-ps pulses with a repetition rate of 76 MHz. The output from the laser is frequency-doubled using a type-II phase-matched KTP crystal and, after separation from the residual infrared by means of a prism, this beam is used as an intense green pump for a second KTP crystal which acts as a traveling-wave parametric amplifier or “paramp.” A small fraction of the infrared beam is also split off to provide a local oscillator for the balanced homodyne detector and a test or “seed” beam which can be recombined with the pump for both alignment purposes and for parametric-gain measurements. Two of the mirrors in the beam lines are mounted on piezoelectric transducers (PZTs) so that the pump and local-oscillator phases can be scanned at frequencies of a few hertz. The pump beam is polarized vertically relative to the horizontal optic axis of the KTP paramp crystal, and hence forms an ordinary wave. Correlated pairs of photons at the fundamental frequency are generated in the form of an ordinary signal beam (S) and an extraordinary idler beam (I). The birefringence of the KTP causes the signal and idler beams to separate or “walk off” spatially, and we use a pair of polarizing-beam-splitter cubes to separate and collinearly recombine the beams to form the composite squeezed mode polarized at 45° to the pump [6]. This squeezed beam is horizontally polarized by means of a half-wave plate and then passes through a prism to separate out the pump. The local oscillator, which is also horizontally polarized, is overlapped both spatially and

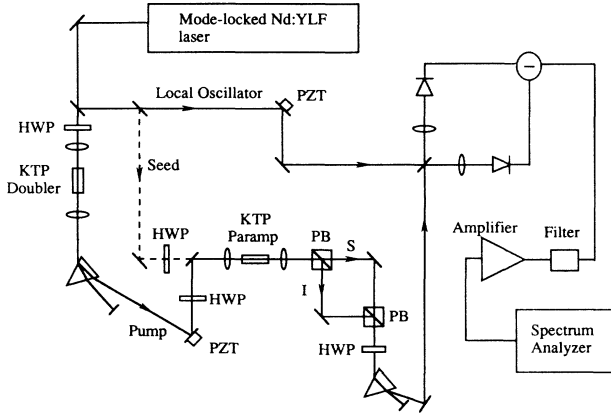


FIG. 1. Experimental setup for squeezing experiments.

temporally with the squeezed beam on a 50:50 beam splitter, and the phase-front matching is carefully optimized.

The homodyne detector consists of the 50:50 beam splitter and a pair of high-quantum-efficiency InGaAs $p-i-n$ photodiodes. The amplified output from this detector is observed in the frequency domain using a spectrum analyzer, and consists of a series of harmonic peaks at 76-MHz intervals with a shot-noise floor in between [14]. The reverse bias for the two photodiodes is of opposite polarity so that the summed output current is in fact the difference photocurrent. By equalizing the path lengths from the beam splitter to the photodiodes it was possible to achieve 30 dB of balancing for the photocurrent harmonics between dc and 0.5 GHz. Very little balancing was observed at frequencies above 1 GHz because of unmatched resonances in the two $P-i-n$ diodes due to stray bond-wire inductances. Consequently, a low-pass filter was used to remove the intense frequency components above 0.5 GHz in order to prevent amplifier saturation. The amplifier has an ac input impedance of 50 Ω and its gain begins to roll off at 0.6 GHz, all of which make it less susceptible to saturation. A prerequisite for the experiments is that the homodyne detector gives shot-noise-limited performance and, as demonstrated in Sec. V, this was found to be true for average photocurrents in the range 0.3–1.0 mA, over the frequency range 0.02–0.5 GHz except within a few megahertz of the harmonic peaks at 76-MHz intervals. Other experiments were also carried out with the photodiode pair positioned after the first polarizing beam splitter, in order to monitor the individual signal and idler beams.

III. GAIN IN THE PARAMETRIC AMPLIFIER

A. Theory of the traveling-wave paramp

The degree of squeezing in the output quantum noise of a parametric amplifier depends explicitly on the magnitude of its gain and, in addition, the gain exhibits the intrinsic phase dependence which is the origin of the squeezing process. Consequently, the gain is an important parameter to investigate. We begin by developing

the traveling-wave theory of the paramp in order to find expressions for the gain which can then be compared with experiment. As discussed by other workers [15,16] the input-output relations for the paramp can be written

$$\hat{a}_{+out}(\omega) = \{ [\cosh s - (i\kappa/\lambda)\sinh s] \hat{a}_{+in}(\omega) - (\beta/\lambda)e^{i\Theta}\sinh s \hat{a}_{-in}^\dagger(\omega_p - \omega) \} \times \exp(ik_+z + ikz), \quad (1)$$

$$\hat{a}_{-out}(\omega) = \{ [\cosh s - (i\kappa/\lambda)\sinh s] \hat{a}_{-in}(\omega) - (\beta/\lambda)e^{i\Theta}\sinh s \hat{a}_{+in}^\dagger(\omega_p - \omega) \} \times \exp(ik_-z + ikz), \quad (2)$$

where $\hat{a}_{in}^\dagger(\omega)$, $\hat{a}_{in}(\omega)$ and $\hat{a}_{out}^\dagger(\omega)$, $\hat{a}_{out}(\omega)$ are continuous-mode creation and destruction operators for the input and output fields,

$$\kappa = \Delta k / 2 = (k_p - k_- - k_+) / 2, \quad (3)$$

$$s = \lambda z, \quad \lambda^2 = \beta^2 - \kappa^2 \quad (\text{for } \beta \geq \kappa). \quad (4)$$

Here, κ is the phase-mismatch parameter which arises from dispersion in the medium [i.e., $k = n(\omega)\omega/c$, where $n(\omega)$ is the frequency-dependent refractive index], β is the gain parameter, z is the length of the paramp, Θ is the pump phase, and the subscripts p , $+$ and $-$, denote the pump and the orthogonally polarized signal and idler modes, respectively. We represent the infrared seed beam at frequency $\omega_p/2$ as a narrow-band coherent state with phase ϕ_{in} , polarized at angle ψ_{in} to the pump polarization direction, and the input signal and idler modes are then excited in continuous-mode coherent states with complex amplitude functions [17]

$$\alpha_{+in}(\omega) = (2\pi F_{in})^{1/2} e^{i\phi_{in}} \cos\psi_{in} \delta[\omega - (\omega_p/2)], \quad (5)$$

$$\alpha_{-in}(\omega) = (2\pi F_{in})^{1/2} e^{i\phi_{in}} \sin\psi_{in} \delta[\omega - (\omega_p/2)], \quad (6)$$

where F_{in} is the total input flux. The total output flux is given by $F_{out} = F_{+out} + F_{-out}$, where the signal flux is

$$F_{+out} = F_{in} | [\cosh s + (i\kappa/\lambda)\sinh s] e^{-i\phi_{in}} \cos\psi_{in} - (\beta/\lambda) e^{-i\Theta + i\phi_{in}} \sinh s \sin\psi_{in} |^2 + (1/2\pi) \int d\omega (\beta/\lambda)^2 \sinh^2 s, \quad (7)$$

and the idler flux F_{-out} is given by a similar expression, but with $\sin\psi_{in}$ and $\cos\psi_{in}$ interchanged. Hence the output fluxes can be written as

$$F_{+out} = G_+(2\phi_{in} - \Theta, \psi_{in}) F_{in} + (1/2\pi) \int d\omega (\beta/\lambda)^2 \sinh^2 s, \quad (8)$$

$$F_{-out} = G_-(2\phi_{in} - \Theta, \psi_{in}) F_{in} + (1/2\pi) \int d\omega (\beta/\lambda)^2 \sinh^2 s, \quad (9)$$

where after some expansion we obtain the gains for general phase and polarization angles

$$G_+(\Phi, \psi) = \cos^2\psi + (\beta/\lambda)^2 \sinh^2 s - 2(\beta/\lambda) \sinh s \sin\psi \cos\psi \times [\cosh s \cos\Phi + (\kappa/\lambda) \sinh s \sin\Phi], \quad (10)$$

and a similar expression for G_- with $\sin\psi$ and $\cos\psi$ interchanged. It can be seen from Eqs. (8)–(10) that the magnitudes of the gains vary with the input polarization angle ψ_{in} , and they are periodic in the relative pump-seed phase $\Phi = (2\phi_{\text{in}} - \Theta)$, except when the input polarization is parallel or perpendicular to the pump (i.e., $\psi_{\text{in}} = 0^\circ$ or 90°). These equations are identical to those obtained using a classical coupled-mode formalism [18], except for the integral terms in Eqs. (8) and (9) which represent the flux of the spontaneously emitted light or, equivalently, the amplified vacuum noise. However, for the purposes of this section we shall ignore these terms since, as shown below, they correspond to nanowatt average power levels in the experiments, while the $G_{\pm} F_{\text{in}}$ terms correspond to the seed power, which is in the milliwatt regime. The extremal values of the gain determined by differentiation of (10) occur at relative phase angles such that

$$\tan\Phi = (\kappa/\lambda) \tanh s \quad (11)$$

and the maximum and minimum gains are

$$G_+(\Phi, \psi)_{\text{max, min}} = \cos^2\psi + (\beta/\lambda^2) \sinh s \times [\beta \sinh s \pm (\beta^2 \cosh^2 s - \kappa^2)^{1/2} \sin 2\psi], \quad (12)$$

with $\cos^2\psi$ replaced by $\sin^2\psi$ in the expression for G_- . The difference between maximum and minimum gains is clearly largest when $\psi = 45^\circ$.

B. Experimental results and discussion

Measurements of parametric gain were carried out by injecting a seed beam at the fundamental frequency codirectionally with the pump. The seed polarization could be varied by means of a half-wave plate, and the relative gains of the signal and idler components were measured using photodiodes placed immediately after the first polarizing beam splitter shown in Fig. 1. The relative pump-seed phase was scanned at a few hertz using the PZT-mounted pump mirror. Figure 2 shows the phase-dependent variation in the average idler photocurrent obtained for an input polarization angle $\psi_{\text{in}} = 45^\circ$. The photocurrent exhibits a periodic oscillation above and below the dc level (dashed line) measured with the pump off. Identical behavior is found for the signal photocurrent at this polarization. This phase-dependent alternation of the gain between amplification and deamplification is well known, and it is a signature of the phenomenon that produces squeezing in the composite signal and idler mode polarized at 45° to the pump. It will be shown in Sec. V that the degree of squeezing depends on the gain parameter β , and this is usually estimated by applying the gain equations (8)–(10) to the gain measured experimentally for one value of ψ_{in} . However, we find that this procedure does not in general give

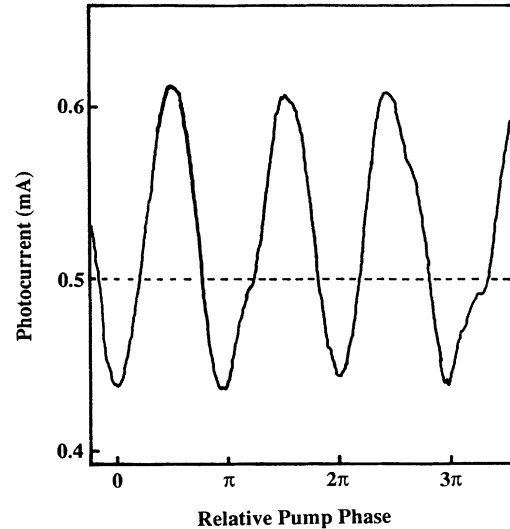


FIG. 2. Average idler photocurrent for input polarization angle $\psi_{\text{in}} = 45^\circ$ as a function of pump phase.

the correct result. For example, in Fig. 3 we plot the maximum and minimum values of the phase-dependent idler gain as a function of input polarization, along with theoretical curves obtained using Eq. (12), with $\kappa \sim 0$ (see Sec. IV), $z = 5 \times 10^{-3}$ m which is the length of the KTP crystal, and $\beta = 30 \text{ m}^{-1}$, which is chosen to match the experimental values at $\psi_{\text{in}} = 0^\circ$. It is evident from the figure that the theory is inadequate at values of $\psi_{\text{in}} \neq 0^\circ$. In particular, the theory predicts that the minimum gain approaches zero for $\psi_{\text{in}}(\text{rad}) \sim \beta z$, whereas the experimental data show only a shallow minimum at this point. The reason for this discrepancy is that the theory assumes perfect spatial and temporal overlap between the pump and the seed pulses, which is not the case in practice. The effects of imperfect overlap can be described approximately by means of an overlap factor m defined such that only a fraction m of the seed pulse intensity experiences the gains given by (10), with the remaining fraction $1 - m$ experiencing no amplification. The effective gain values are consequently changed to

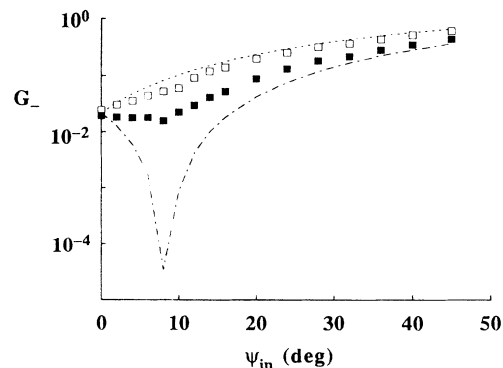


FIG. 3. The points show the maximum and minimum values of idler gain G_- measured as a function of input polarization. The dashed lines show the theoretical variation obtained by assuming perfect pump-seed overlap.

$$G_{m+} = mG_+ + (1-m)\cos^2\psi_{in}, \quad (13)$$

$$G_{m-} = mG_- + (1-m)\sin^2\psi_{in}, \quad (14)$$

where the plus and minus subscripts denote signal and idler as previously. Figure 4 shows a fit to the data obtained using the revised gain expressions, where the optimized β and m values are 54 and 0.29 m^{-1} respectively. Although this process involves two parameters, we do obtain a well-defined best fit with a unique pair of β and m values and find, in addition, that a change in β of $\pm 15\%$ is enough to make the fit noticeably poor for all values of m . A further justification of the procedure is that if the seed and pump beams are deliberately misaligned so that the experimentally measured gains are further reduced, the fit to the data gives a β value in the same range but with a lower m value. For comparison, using the measured pump intensity of $\sim 40 \text{ MW/cm}^2$ and the nonlinear susceptibility of KTP [19], we predict [18] a value of $\beta = 70 \text{ m}^{-1}$, which is in reasonable agreement with the experimental result. The overlap factor is probably limited by the effects of birefringent walkoff in the doubling and the paramp crystals, and by imperfect pump and seed beam collimations which lead to nonideal focusing conditions. In summary we find $\beta \sim \lambda = 54 \text{ m}^{-1}$, $s = \lambda z = 0.27$, and we calculate the minimum total gain ($G_+ + G_-$) for an input polarization of 45° to be 0.58 or -2.3 dB . The magnitude of the calculated gain thus lies below the value of 3 dB that marks the onset of the spatial distortion effects considered by La Porta and Slusher [20].

IV. PHASE MATCHING AND SPONTANEOUS FLUORESCENCE

A. Phase matching

In a practical KTP parametric amplifier, phase mismatch between the coupled pump, signal, and idler waves arises from dispersion in the crystal and limits the frequency range over which gain can occur. In Sec. III, we developed a plane-wave theory to describe the amplification process for monochromatic pump and seed beam. However, in practice, both pump and seed beams

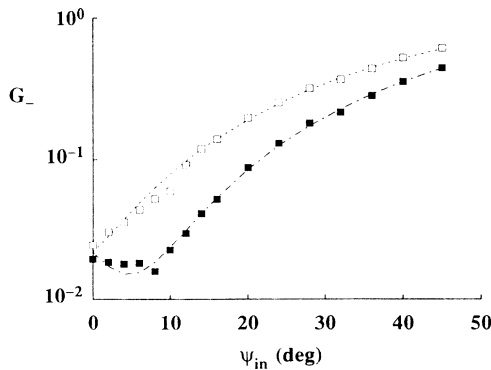


FIG. 4. The points are the experimental data for the idler gain from Fig. 3. The dashed lines are a fit to the data using the theory with imperfect pump-seed overlap.

are pulsed and therefore nonmonochromatic, and they take the form of focused Gaussian beams rather than infinite plane waves. Therefore it is important to estimate whether the plane-wave theory is applicable, and if so, what value of phase mismatch parameter is appropriate for the calculations. Some insight into this problem can be obtained by calculating the phase-matching conditions for parametric amplification from the published refractive-index data for KTP [19]. KTP is biaxially birefringent, and the propagation direction for type-II phase matching is in the $x-y$ plane perpendicular to the primary optic axis which lies in the z direction (see inset to Fig. 5). The pump and signal waves are polarized parallel to the $x-y$ plane (ordinary) and have wave vectors whose magnitudes vary with the propagation direction which is defined by the angle γ . In contrast, the idler wave is polarized parallel to the z axis (extraordinary) and has a wave vector whose magnitude is independent of γ . The difference between the n_x and n_y indices is sufficiently large to allow phase matching over a wide range of wavelengths by varying γ . However, since n_z is significantly larger than n_x and n_y , KTP can be treated as effectively uniaxial, and the terms, ordinary and extraordinary are used to define the polarization directions. Phase matching occurs when γ is chosen such that pump, signal, and idler indices satisfy

$$2n_p(\gamma) = n_+(\gamma) + n_-, \quad (15)$$

where $n(\gamma)$ is given by the index ellipsoid

$$n(\gamma)^{-2} = (\cos^2\gamma)/n_y^2 + (\sin^2\gamma)/n_x^2. \quad (16)$$

Using the wavelength-dependent Sellmeier equations derived by Fan *et al.* [19] for the refractive-index components n_x, n_y , and n_z in KTP, we calculate $\gamma = 32.95^\circ$ for degenerate phase matching (i.e., pump wavelength equal to 526.5 nm, signal and idler wavelengths equal to 1053 nm). In order to investigate the effect of a finite spread in frequencies for the signal and idler waves, we write the phase-mismatch parameter as

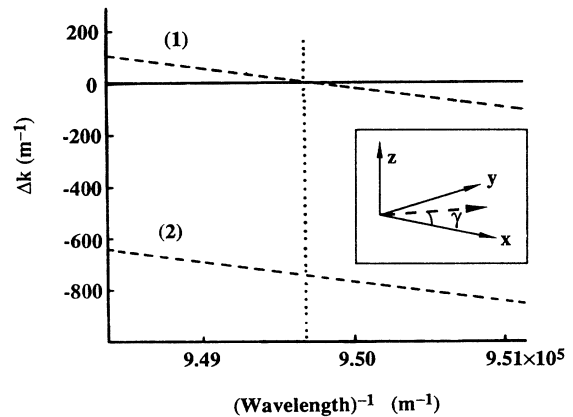


FIG. 5. Calculated variation in phase-mismatch parameter Δk with wave number. Results are shown for (1) $\gamma = 32.95^\circ$ and (2) $\gamma = 33.51^\circ$, where γ defines the propagation direction, as shown in the inset to the figure. The vertical dotted line indicates the position of the degeneracy frequency.

$$\Delta k = k_p(\omega_p) - k_+(\omega_p/2 + \epsilon) - k_-(\omega_p/2 - \epsilon), \quad (17)$$

where the signal and idler frequencies are displaced by an amount ϵ on either side of the degeneracy frequency $\omega_p/2$ [16]. Using the refractive-index data for KTP, we calculate numerically the Δk given by Eq. (17). The results of these calculations are shown in Fig. 5, plotted against wave number. Note that although Δk can be either positive or negative, we are only concerned with the magnitude of Δk , and in what follows we drop the modulus signs for simplicity. The results can now be compared with the experimental case of seeded parametric amplification, where we assume transform-limited 50-ps seed pulses which leads to a full width at half maximum (FWHM) spread in wavelength of 2.3×10^{-2} nm or, alternatively, to a wave-number spread of 21 m^{-1} . It can be seen from curve 1 in Fig. 5 that this spread leads to only very small values of phase mismatch, i.e., $\Delta k \sim 0.8 \text{ m}^{-1}$ at the FWHM points. This is negligible compared with the value for the gain parameter $\beta = 54 \text{ m}^{-1}$, which was obtained from experiment. Although we have only considered the spread in seed frequencies up to this point, the spread in pump frequencies similarly leads to negligible levels of phase mismatch.

In contrast, focusing the Gaussian pump and seed beams does lead to large values of phase mismatch in the experiment. This can be illustrated by considering pump, signal, and idler waves propagating at some angle, ξ , to the direction for degenerate phase matching ($\gamma = 32.95^\circ$). If ξ is chosen as the diffraction angle appropriate for the degree of focusing present in the experiment, then this represents the most strongly divergent part of the focused beams. In this case

$$\xi = \rho / \pi \omega n, \quad (18)$$

where ρ and n are the wavelength and index appropriate for the seed beam, and $\omega = 19 \text{ } \mu\text{m}$ is the radius of the beam waist measured at the focal point of the seed beam. This leads to a value of $\xi = 0.56^\circ$. We then use Eqs. (16) and (17) to calculate the phase mismatch as a function of wave number for a propagation angle $(\xi + \gamma) = 33.51^\circ$. The results are shown as curve 2 in Fig. 5. It can be seen that Δk is $\sim 750 \text{ m}^{-1}$ at the seed frequency which is now much larger than the gain parameter $\beta = 54 \text{ m}^{-1}$.

Despite this previous finding, we argue that the Δk that appears in the plane-wave theory should in fact be small. The deduction follows from the theory of parametric interactions of focused Gaussian beams developed by Boyd and Kleinman [21]. For example, in the case of second-harmonic generation by focused beams, the maximum conversion efficiency is always obtained with $\Delta k > 0$ for the on-axis beam. For comparison, for a KTP crystal of length $5 \times 10^{-3} \text{ m}$, this theory predicts an optimum Δk value of 620 m^{-1} , which is similar to the value obtained above. Most importantly, under such optimum focusing conditions, the conversion process is formally equivalent to the case of perfectly phase-matched plane waves. This is a consequence of the fact that, if $\Delta k > 0$ for wave vectors parallel to the axis of the diverging beam, phase matching is nevertheless possible with other non-axial wave vectors. Such noncollinear mixing pro-

cesses are not possible for $\Delta k = 0$. Consequently, despite the large Δk values produced by focusing in the experiment, we are justified in taking the approximation $\Delta k \ll \beta$, in our equivalent plane-wave theory, and in fact in Sec. III B we took the limit $\kappa = \Delta k / 2 = 0$.

We find that the gain calculated from our plane-wave theory is relatively insensitive to the Δk value unless $\Delta k \gg \beta$. This is evident if we consider the theory of Sec. III A, now with $\Delta k \geq \beta$. The hyperbolic terms such as $\sinh^2 s$ in the expression for the gain given by Eq. (10) are then replaced by periodic terms such as $\sin^2 s$. This means that for large values of s no sustained growth of the signal and idler waves is possible along the length of the crystal and the gain is consequently reduced. However, since the crystal is relatively short in this experiment, i.e., $z = 5 \times 10^{-3} \text{ m}$, s is small even for values of Δk significantly larger than β , and the gain is approximately the same as in the $\Delta k = 0$ limit. This can be seen from Fig. 6, where we plot the gain calculated using Eq. (10) and its $\Delta k \geq \beta$ form, versus $\kappa = \Delta k / 2$. The gain is approximately constant up to Δk values of order 5β , at which point $s \sim \pi/4$. This further shows that our assumption of $\kappa = \Delta k / 2 = 0$ in Sec. III B is justified, since Δk has only a small effect on the calculated gain.

B. Spontaneous parametric fluorescence

We have already seen from Eqs. (8) and (9) that the paramp also generates output flux even when there is no seed input. This spontaneous parametric fluorescence can be viewed as arising from amplification of the vacuum or quantum fluctuations. Since the quantum noise, unlike the seed beam, is ultrabroad band in nature, the paramp could in principle produce spontaneous output flux over a correspondingly broad frequency range, as long as the correlated photon pairs in the signal and idler modes satisfy conservation of energy, i.e., $\omega_p = \omega_- + \omega_+$. However, as discussed above, this frequency bandwidth is ultimately limited by phase mismatch.

In order to investigate this process, the spectrum of the spontaneous parametric fluorescence was measured using a scanning monochromator and a germanium photodiode. These were positioned after the paramp output lens, which was then adjusted to focus the spontaneous light onto the input slit of the monochromator. The

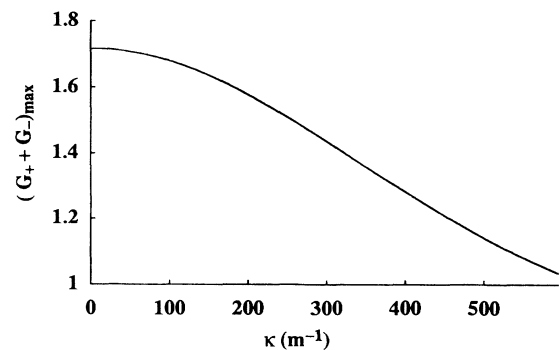


FIG. 6. Maximum value of the total paramp gain calculated as a function of the phase-matching parameter $\kappa = \Delta k / 2$.

pump beam was mechanically chopped, and synchronous detection was used to measure the spontaneous signal at each wavelength. Since the spontaneous process is only phase matched for the ordinary polarization of the pump, spectra were obtained for both ordinary and extraordinary polarizations and subtracted in order to remove unwanted background signal arising from filter fluorescence etc. The spectra were then normalized for detector response and monochromator throughput using a calibrated white-light source. The results of this procedure are shown in Fig. 7, plotted against wave number. The sharp spike at the degeneracy point is an experimental artifact that arises from a very small amount of residual scattered infrared radiation which is focused onto the slits of the monochromator by the paramp output lens. Apart from this artifact, the spectrum is very broad with a FWHM of about $1.2 \times 10^5 \text{ m}^{-1}$, which corresponds to a frequency spread of about 36 THz. Measurements were also performed using a calibrated power meter and with the monochromator removed in order to measure the total emitted power. This was found to be of the order of 6 nW for an average pump power of 0.8 W.

As discussed in the following section, the intrinsic phase dependence of the paramp produces quadrature squeezing in the amplified quantum noise, and the spectral measurements above show that this can extend over many terahertz. However, this huge frequency range will

not all be accessible experimentally, since, as discussed by Huttner, Serulnik, and Ben-Aryeh [16] away from the degeneracy point the phase of the squeezed quadrature varies with frequency, and therefore cannot be observed for a single local-oscillator-phase setting. In addition, since phase matching causes different frequencies to be emitted at different angles, the experiment acts as a spatial filter, and only those frequency components that have the same spatial mode as the local oscillator contribute efficiently to the measured noise reduction. This effect is accentuated by dispersion in the output lens, which means that only those frequencies close to the degeneracy frequency in the output beam can be collimated effectively and mixed with the local oscillator.

V. VACUUM-NOISE SQUEEZING

A. Theory

We now consider theoretically the case discussed in Sec. IV B above, that is to say the parametric amplifier with the seed beam removed ($F_{\text{in}}=0$), so that the output consists only of the amplified vacuum input noise. Measurements of the output noise by balanced-homodyne detection are represented by the dimensionless field operator [17,22].

$$\hat{E}(\phi_L) = (2\pi T)^{-1/2} \int_{\tau}^{\tau+T} dt \int d\omega \{ i\hat{a}_{\text{out}}^{\dagger}(\omega) \exp[i(\omega - \omega_p/2)t + i\phi_L] - i\hat{a}_{\text{out}}(\omega) \exp[-i(\omega - \omega_p/2)t - i\phi_L] \}, \quad (19)$$

where T is the integration time, with the period of detection extending from time τ to time $\tau+T$, ϕ_L is the phase of the local oscillator, and the frequency of the local oscillator is one half of the pump frequency ω_p . It is essential for the observation of phase-dependent noise that the homodyne detector receives contributions from both the signal and idler (plus and minus) modes of the paramp. The output operator in (19) is given by

$$\hat{a}_{\text{out}}(\omega) = \hat{a}_{+\text{out}}(\omega) \cos\psi_{\text{out}} + \hat{a}_{-\text{out}}(\omega) \sin\psi_{\text{out}}, \quad (20)$$

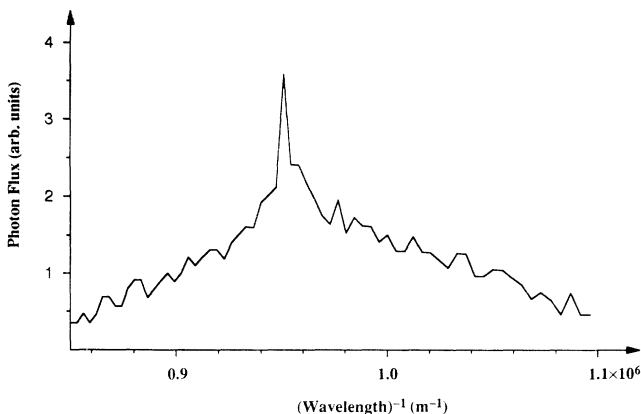


FIG. 7. The measured spontaneous-parametric-fluorescence spectrum.

when the signal and idler modes are overlapped (spatially and temporally) to form a composite mode linearly polarized at angle ψ_{out} to the signal mode polarization direction. The expression (19) is valid only for detection bandwidths that are small compared to $\omega_p/2$.

The mean and the variance of the homodyne field are now obtained straightforwardly by substitution of (1) and (2) into (20), and (20) into (19). The results are thus expressed in terms of expectation values of the input operators. For a vacuum input

$$\langle \hat{E}(\phi_L) \rangle = 0 \quad (21)$$

and

$$\begin{aligned} \langle [\Delta \hat{E}(\phi_L)]^2 \rangle &= G_+(\pi - 2\phi_L + \Theta, \psi_{\text{out}}) \\ &\quad + G_-(\pi - 2\phi_L + \Theta, \psi_{\text{out}}), \end{aligned} \quad (22)$$

where the plus and minus mode gains are defined in (10). In the absence of the parametric amplifier, (22) reduces to

$$\langle [\Delta \hat{E}(\phi_L)]^2 \rangle = 1 \quad (\text{i.e., for } s=0), \quad (23)$$

and this represents the standard quantum limit or shot noise that ordinarily occurs in homodyne detection. Any squeezing produced by the presence of the parametric amplifier is characterized by a variance smaller than unity. According to (11), the minimum variance occurs for local oscillator phase angles ϕ_L such that

$$\tan(2\phi_L - \Theta) = -(\kappa/\lambda)\tan\hs \quad (24)$$

and for 45° output polarization, when (12) gives

$$\begin{aligned} \langle [\Delta\hat{E}(\phi_L)]^2 \rangle_{\min} \\ = 1 + (2\beta/\lambda^2)\sinh s [\beta \sinh s - (\beta^2 \cosh^2 s - \kappa^2)^{1/2}]. \end{aligned} \quad (25)$$

The homodyne variances calculated above are intrinsic values that could in principle be observed in a lossless system with ideal detectors. The effects of loss and detector quantum efficiencies smaller than unity can be incorporated in the theory by replacing the output operators defined in (1) and (2) by detector operators [23]

$$\hat{d}_+(\omega) = \eta_+^{1/2} \hat{a}_{+\text{out}}(\omega) + i(1 - \eta_+)^{1/2} \hat{v}_+(\omega), \quad (26)$$

$$\hat{d}_-(\omega) = \eta_-^{1/2} \hat{a}_{-\text{out}}(\omega) + i(1 - \eta_-)^{1/2} \hat{v}_-(\omega), \quad (27)$$

where η_+ and η_- are loss factors, whose natures are discussed in Sec. V B, and the \hat{v} operators represent vacuum fields that are coupled into the detected light beams by the loss processes. For a perfectly balanced detection system $\eta_+ = \eta_- = \eta$, and the measured homodyne variance is proportional to

$$\langle [\Delta\hat{E}(\phi_L)]^2 \rangle_{\text{meas}} = \eta \langle [\Delta\hat{E}(\phi_L)]^2 \rangle + 1 - \eta, \quad (28)$$

where the constant of proportionality is the mean number of detected local-oscillator photons in time T .

B. Experimental results and discussion

In order to observe squeezing effects it is necessary to ensure that the homodyne detector gives shot-noise-limited performance when there is no input to its signal port. As a first step, with the local oscillator off, we check that the gain of the electronic amplifier is sufficiently high to bring the detector's thermal output noise several decibels above the spectrum analyzer noise floor. When the local oscillator power is increased, the total noise level rises above the thermal noise due to the contribution of broadband shot noise. The shot noise is expected to vary linearly with average photodiode current [14] i_{av} and this behavior is well illustrated in Fig. 8, where we plot the noise power measured at 440 MHz against i_{av} (the spectrum-analyzer-resolution bandwidth was 100 kHz, and the measured thermal noise of -102 dBm was subtracted). This linear dependence of the shot noise can be contrasted with the behavior of the partially balanced photocurrent harmonics at 76-MHz intervals. The peak power of these harmonics varies as i_{av}^2 as illustrated in Fig. 8 for the 456-MHz peak. This confirms that the noise measured at 440 MHz is Poissonian in nature, and does not arise from a harmonic side band, for example. However, the main tests that the noise level is indeed due to shot noise are that it is within a few percent of the theoretical value and, in addition, is truly broadband, since as the local oscillator power is increased the noise floor between the photocurrent harmonics is observed to increase uniformly across the entire accessible frequency range of 0.02–0.5 GHz. It was also found that for photocurrents above 1 mA the noise in-

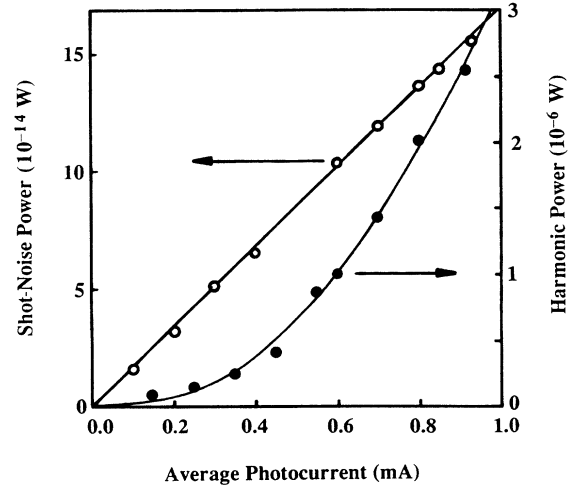


FIG. 8. Variation of shot-noise power (open circles) and harmonic power (solid circles) with average photodiode current. Thermal noise of 6.3×10^{-14} W was subtracted from the total measured noise to obtain the shot-noise contribution. Typical error bars are represented by the size of the circles.

creased rapidly and nonlinearly due to saturation of both the photodiode response and the electronic amplifier, consequently i_{av} was always kept below this limit.

When the output from the parametric amplifier is directed into the signal port of the homodyne detector the noise level between photocurrent harmonics becomes a function of local oscillator phase, as shown in Fig. 9 for a frequency of 440 MHz. The noise maxima and minima are approximately 0.7 dB (17.5%) above and 0.5 dB (11%) below the combined shot noise and thermal noise level measured with the paramp output blocked. The average photocurrent is 0.66 mA, and the combined noise level is -97.2 dBm, which is 4.8 dB above the thermal noise. Taking into account the contribution of the thermal noise, we find that measured shot-noise reduction due to squeezing is ~ 0.8 dB or 17%. Since losses in the experiment add uncorrelated noise which degrades the degree of squeezing, this value is smaller than the maximum level of noise reduction achieved by the paramp. As shown by Eq. (25), this is given by the minimum gain value for polarization angle $\psi = 45^\circ$, which in Sec. III B was found to be equal to 0.58. This predicts 2.3 dB or 42% of squeezing in an ideal lossless experiment. The measured and minimum levels of squeezing are related by Eq. (28), in which η , the total loss, is the product of several components given by

$$\eta = \eta_d \eta_o \eta_h. \quad (29)$$

Here, $\eta_d = 0.89$ is the detector quantum efficiency, $\eta_o = 0.82$ is due to reflection and absorption loss in the optical path after the paramp, and η_h is the homodyne mode-matching efficiency for the squeezed beam and the local oscillator. The parameter η_h is difficult to measure experimentally, but the upper limit is about 0.8 since, even with perfect temporal overlap, there are spatial differences in the modes due to the nonlinear generation mechanism for the squeezed beam [5,7]. Consequently,

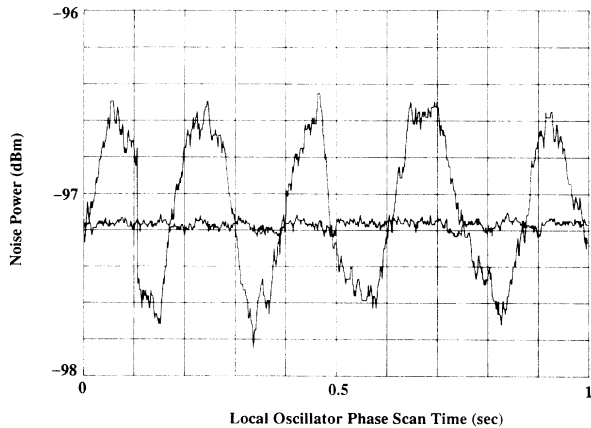


FIG. 9. Homodyne detector noise measured as a function of local oscillator phase. The two traces show the phase-independence noise level obtained with the paramp output off and the phase-dependent noise obtained with the paramp output on. The maximum noise reduction due to squeezing is about 0.5 dB.

we take the approach of using Eq. (28) to estimate the total loss parameter η , and then check that this gives an acceptable value for η_h using Eq. (29). This process leads to estimates of $\eta=0.39$ and $\eta_h=0.53$. In order to see whether this low value for η_h is reasonable, an experiment was carried out to measure the mode-matching efficiency of the seed beam with the local oscillator. In an ideal experiment this mode-matching efficiency should be unity since the two beams are derived from the same source. The measurement is straightforward, since the seed power can be made comparable to the local oscillator power, so that when the phase of the local oscillator is scanned, the strong interference between the two beams produces large swings in the average photodiode currents. The depth of this modulation can be directly related to the seed-local oscillator mode-matching efficiency, denoted as η'_h , and we obtain a maximum value of $\eta'_h=0.65$. This value is less than unity because, although the seed and local oscillator are generated from the same laser, there are many optical components in the optical paths which can produce phase front distortions and slightly different divergences for the beams. Now, by comparison, we see that the low value of $\eta_h=0.53$ obtained for the mode-matching efficiency of the squeezed vacuum and the local oscillator is reasonable. Moreover, since the ratio $(\eta_h/\eta'_h)=0.81$, the mode-matching efficiency is in fact close to the optimum value discussed above. In conclusion, we also note that if the overlap factor m had not been included in the gain calculation in Sec. III B, we would have obtained the smaller value for the gain parameter β of 30 m^{-1} , which leads to the far-too-large estimate of $\eta_h=0.89$.

VI. INTENSITY NOISE REDUCTION IN DIFFERENCE PHOTODETECTION

A. Theory

In addition to quadrature squeezing of the vacuum noise, another aspect of the nonclassical behavior of the

paramp is that the difference in the intensity fluctuations between the signal and idler also exhibits squeezing [8,11–13]. This occurs because the signal and idler photons are created pairwise and hence the intensity fluctuations are strongly correlated. As has been pointed out previously [11], this can be seen from the equality of the operators that represent the difference output flux $F_{+out} - F_{-out}$ and the difference input flux $F_{+in} - F_{-in}$. The input and output difference fluxes thus have the same noise characteristics, and these can be studied by direct detection of the two output modes. With the coherent input seed beam at frequency $\omega_p/2$ described by (5) and (6) now restored, the difference in output fluxes is readily obtained from (8) and (9). However, it is necessary to rework the calculation replacing the output operators (1) and (2) by the detector operators (26) and (27) to allow for loss and imperfect quantum efficiencies, as in (29). If the total loss factors for the two output modes are both equal to η , the mean measured difference in output fluxes for a detector integration time T is

$$\begin{aligned} \langle \hat{D}_{out} \rangle &= \eta [G_+(2\phi_{in} - \Theta, \psi_{in}) \\ &\quad - G_-(2\phi_{in} - \Theta, \psi_{in})] F_{in} T \\ &= \eta F_{in} T \cos 2\psi_{in}. \end{aligned} \quad (30)$$

The mean vanishes for an input polarization angle of 45° , and in this case the variance in the measured difference in output fluxes is

$$\begin{aligned} \langle (\Delta \hat{D}_{out})^2 \rangle &= \eta(1-\eta) [G_+(2\phi_{in} - \Theta, \pi/4) \\ &\quad + G_-(2\phi_{in} - \Theta, \pi/4)] F_{in} T \\ &\quad + \eta^2 F_{in} T, \end{aligned} \quad (31)$$

where we omit the negligible amplified-vacuum-noise term [see Eqs. (8) and (9)]. From Eq. (10) the sum of the gains is

$$\begin{aligned} G_+ + G_- &= 1 + 2(\beta/\lambda)^2 \sinh^2 s - (2\beta/\lambda) \sinh s \\ &\quad \times [\cosh s \cos(2\phi_{in} - \Theta) \\ &\quad + (\kappa/\lambda) \sinh s \sin(2\phi_{in} - \Theta)]. \end{aligned} \quad (32)$$

It can be seen from (31) and (32) that in a lossless experiment ($\eta=1$), although the individual signal and idler photocurrents vary with pump phase Θ , the difference-photocurrent noise is phase independent and, as discussed above, is the same as that obtained with the pump off. In contrast, if the signal and idler were totally uncorrelated, the quantum noise on the difference photocurrent would simply be the sum of the noises on the individual signal and idler photocurrents, and therefore would have the same phase dependence. Hence the paramp either amplifies the signal and idler modes by adding pairs of strongly correlated photons, which do not increase the difference-intensity noise, or deamplifies the signal and idler modes by removing photons pairwise, which maintains the difference-intensity noise at its input value. In Sec. VI B, we investigate experimentally the transition between the correlated and uncorrelated behavior by introducing excess loss into the system.

B. Experimental results and discussion

Difference-photocurrent measurements were performed by placing the photodiodes in the signal and idler beams directly after the first polarizing beam splitter shown in Fig. 1. Brewster-angled glass filters were used to remove the pump from the paramp output, and the seed power was set so that the signal and idler photocurrents were both equal to 0.54 mA when the pump was off. Under these conditions, the noise measured on the spectrum analyzer was shot-noise dominated, and the maximum photocurrent levels obtained in the experiment were below the detector saturation level. When the pump was turned on, and its phase scanned, the signal and idler photocurrents varied as shown in Fig. 2, and the maximum and minimum values of paramp gain were as illustrated in Fig. 3 for $\psi_{in} = 45^\circ$. Figure 10(a) shows the total noise measured at 440 MHz under these conditions as a function of pump phase. We find a residual phase dependence which is consistent with the unavoidable loss in the experiment. This is due to the transmission of the filters (0.96) and the quantum efficiency of the photodiodes (0.89) which give a total loss coefficient $\eta = 0.85$. The loss in the experiment was then increased by placing absorbing filters after the paramp. In each case the seed power was increased so that the signal and idler photocurrents remained the same in order to ensure that the ratio of the shot noise to the thermal noise remained constant. The results are shown in Figs. 10(b) and 10(c) for loss coefficient values of 0.43 and 0.16, respectively. We find progressively more phase dependence in the output noise as the correlations in the paramp output are destroyed by the increased loss, and the results are well modeled by Eq. (31). From a comparison of Figs. 10(a) and 10(c) it can be seen that the experiment produces about 0.6 dB of total noise reduction in the lowest loss situation.

VII. SUMMARY AND CONCLUSION

In conclusion, we have used pulsed parametric amplification in KTP to investigate both quadrature squeezing via phase-sensitive homodyne detection, and also "twin-beam" noise reduction using direct-detection techniques. The quadrature squeezing experiment produced total noise reductions ~ 0.5 dB (11%), corresponding to ~ 0.8 dB (17%) of quantum-noise reduction, at frequencies up to 0.5 GHz. These results were modeled using a multimode traveling-wave theory, and consistent values of the parameters describing gain, loss, and mode

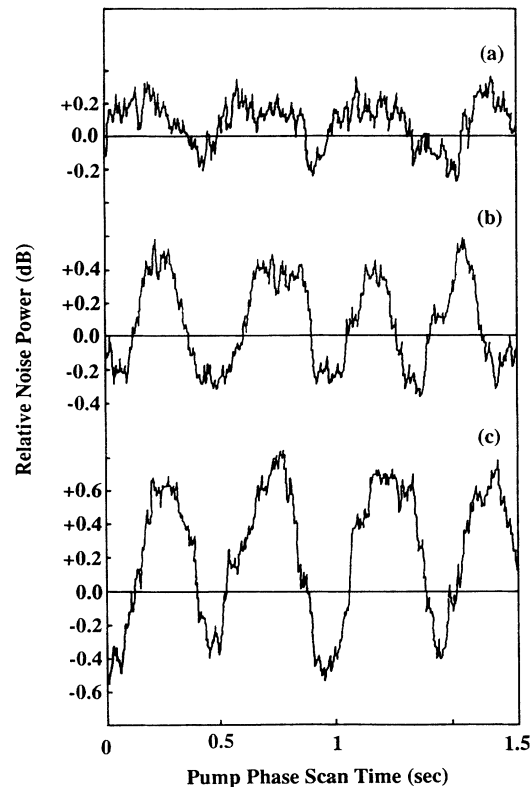


FIG. 10. Ratio of the difference-photocurrent noise obtained with the pump on to that obtained with the pump off, measured as a function of pump phase. The output loss increases from (a) to (c).

mismatch were determined. In the twin-beam experiment, the transition between correlated and uncorrelated behavior of the paramp was investigated by the introduction of excess loss and modeled using the traveling-wave theory.

ACKNOWLEDGMENTS

We thank K. J. Blow and S. J. D. Phoenix for important discussions regarding the theory of parametric amplifiers, and J. K. Lucek for help with the experimental setup. In addition, we thank the Devices Research Division and Technology Research Division at BT Laboratories for the provision of high-quantum-efficiency photodiodes and help with homodyne-detector design, respectively.

*Permanent address: Physics Department, Essex University, Colchester CO4 3SQ, United Kingdom.

- [1] See, for example, R. Loudon, and P. L. Knight, *J. Mod. Opt.* **34**, 709 (1987).
- [2] R. E. Slusher, L. W. Hollberg, B. Yurke, J. C. Mertz, and J. F. Valley, *Phys. Rev. Lett.* **55**, 2409 (1985).
- [3] R. M. Shelby, M. D. Levenson, S. H. Perlmutter, R. G. DeVoe, and D. F. Walls, *Phys. Rev. Lett.* **57**, 691 (1986).
- [4] Ling-An Wu, H. J. Kimble, J. L. Hall, and Huifa Wu, *Phys. Rev. Lett.* **57**, 2520 (1986).
- [5] R. E. Slusher, P. Grangier, A. LaPorta, B. Yurke, and M. J. Potasek, *Phys. Rev. Lett.* **59**, 2566 (1987).
- [6] P. Kumar, O. Aytur, and Jianming Huang, *Phys. Rev. Lett.* **64**, 1015 (1990).
- [7] T. Hirano and M. Matsuoka, *Opt. Lett.* **15**, 1153 (1990).
- [8] C. D. Nabors and R. M. Shelby, *Phys. Rev. A* **42**, 556 (1990).
- [9] P. Grangier, R. E. Slusher, B. Yurke, and A. LaPorta, *Phys. Rev. Lett.* **59**, 2153 (1987).
- [10] Min Xiao, Ling-An Wu, and H. J. Kimble, *Phys. Rev.*

- Lett. **59**, 278 (1987).
- [11] O. Aytur and P. Kumar, Phys. Rev. Lett. **65**, 1551 (1990).
- [12] A. Heidmann, R. J. Horowicz, S. Reynaud, E. Giacobino, and C. Fabre, Phys. Rev. Lett. **59**, 2555 (1987).
- [13] T. Debuisschert, S. Reynaud, A. Heidmann, E. Giacobino, and C. Fabre, Quantum Opt. **1**, 3 (1989).
- [14] B. Yurke, P. Grangier, R. E. Slusher, and M. J. Potasek, Phys. Rev. A **35**, 3586 (1987).
- [15] D. D. Crouch, Phys. Rev. A **38**, 508 (1988).
- [16] B. Huttner, S. Serulnik, and Y. Ben-Aryeh, Phys. Rev. A **42**, 5594 (1990).
- [17] K. J. Blow, R. Loudon, S. J. D. Phoenix, and T. J. Shepherd, Phys. Rev. A **42**, 4102 (1990).
- [18] A. Yariv, *Optical Electronics*, 3rd ed. (Holt, Rinehart and Winston, New York, 1985).
- [19] T. Y. Fan, C. E. Huang, B. Q. Hu, R. C. Eckardt, Y. X. Fan, R. L. Byer, and R. S. Feigelson, Appl. Opt. **26**, 2390 (1987); R. C. Eckardt, H. Masuda, Y. X. Fan, and R. L. Byer, IEEE J. Quantum Electron. **26**, 922 (1990).
- [20] A. LaPorta and R. E. Slusher, Phys. Rev. A **44**, 2013 (1991).
- [21] G. D. Boyd and D. A. Kleinman, J. Appl. Phys. **39**, 3597 (1968).
- [22] M. J. Collett, R. Loudon, and C. W. Gardiner, J. Mod. Opt. **34**, 881 (1987).
- [23] H. P. Yuen and J. H. Shapiro, IEEE Trans. Inf. Theory **26**, 78 (1980).